Improving Microresonators Reliability in Silicon Photonic Integrated Circuits

Mahdi Nikdast[1], Gabriela Nicolescu[2], and Odile Liboiron-Ladouceur[3]
[1]Colorado State University, CO, USA [2]Polytechnique Montréal, QC, Canada [3]McGill University, QC, Canada

***Abstract*—Exploring microresonators (MRs) design space, we demonstrate a design method (DeEPeR) to enhance MRs reliability in silicon photonic integrated circuits (PICs) under fabrication process variations. DeEPeR is validated through fabricating several MRs. Moreover, simulation results indicate considerable optical signal-to-noise ratio improvements in PICs using DeEPeR.**

I. Introduction

Microresonators (MRs), which are widely employed in silicon photonic integrated circuits (PICs), are considerably sensitive to fabrication process variations (PV). Particularly, such variations deviate the resonant wavelength of MRs [1], resulting in performance and reliability degradation in PICs utilizing MRs for modulating, filtering, and switching optical signals. Silicon-on-insulator (SOI) thickness and waveguide width variations, considered in this work, are the major concerns in silicon photonics fabrications. Several methods have been proposed to compensate for PV, and specifically to restore the resonant wavelength of MRs, including those based on applying high-energy particles (e.g., UV light), but at a cost of degrading MRs quality factor, and also trimming techniques (e.g., thermal tuning), which are power hungry and often have a limited correction range.

This paper demonstrates an efficient device-level design method, called DeEPeR, to improve MRs reliability in PICs under PV. Considering different range of variations, DeEPeR explores the design space of MRs to study how employing different design parameters in such components impacts the resonant wavelength shift, and hence MRs performance and reliability. Also, our study includes the design and fabrication of several MRs using DeEPeR for experimental validation. Indicating the impact of DeEPeR in PICs, we apply our method to a case study of a wavelength division multiplexed (WDM) optical filter, in which we show how the optical signal-to-noise ratio (OSNR) considerably improves (5.2 dB on average) when using DeEPeR. The OSNR determines the received optical signal quality and the bit error rate (BER) in a system, hence denoting the performance and reliability.

II. DeEPeR: Design Exploration and Guidelines

Fig. 1(a) indicates cross sections of two strip (or ridge) waveguides in proximity with a gap of g (coupling region in the MR). We consider symmetric waveguides with a silicon (Si) core buried in silicon dioxide (SiO_2). The SOI thickness ($t = t_{w,MR}$) depends on the wafer thickness standard and cannot be altered during the design process. Also, the ridge thickness (t_r), and hence the slab thickness (t_{sl}), in ridge waveguides depends on the available etching depths in

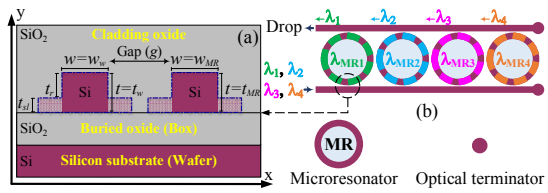

Fig. 1. (a) Cross sections of two strip (solid) or ridge (dashed) waveguides in proximity; and, (b) A passive WDM add-drop filter.

the fabrication process. Nevertheless, the waveguide width ($w = w_{w,MR}$) can be determined during the design time. The resonant wavelength in MRs (λ_{MR}) highly depends on w and t, both of which are susceptible to PV, imposing resonant wavelength shifts ($\Delta\lambda_{MR}$) in MRs. Readers can refer to the method proposed in [2] to calculate $\Delta\lambda_{MR}$.

As λ_{MR} changes almost linearly with the variations in w and t, we can define the $\Delta\lambda_{MR}$ slope when, for example, w varies ($\frac{\partial\lambda_{MR}}{\partial w}$) as $|\frac{\Delta\lambda_{MR}(\lambda,w+\nu_w,t)-\Delta\lambda_{MR}(\lambda,w-\nu_w,t)}{2\nu_w}|$, where ν_w denotes the variations in w. Similarly, we can define $\frac{\partial\lambda_{MR}}{\partial t_r,t}$, which are $\Delta\lambda_{MR}$ slopes with respect to the variations in t_r and t. Considering $\frac{\partial\lambda_{MR}}{\partial w,t_r,t}$ and the standard deviations associated with the variations in w (σ_w), t_r (σ_{t_r}), and t (σ_t), the total $\Delta\lambda_{MR}$ ($\Delta^T\lambda_{MR}$) in an MR is defined as $\sigma_t(\frac{\partial\lambda_{MR}}{\partial w}\alpha_{p/a} + \frac{\partial\lambda_{MR}}{\partial t_r}\alpha_a + \frac{\partial\lambda_{MR}}{\partial t})$. Here, we have $\alpha_p = \frac{\sigma_w}{\sigma_t}$ and $\alpha_a = \frac{\sigma_w+\sigma_{t_r}}{2\sigma_t}$, in which the arithmetic mean between σ_w and σ_{t_r} is considered for α_a. The subscripts p and a denote the use of passive (based on strip waveguides) and active (based on ridge waveguides) MRs, respectively (see Fig. 2).

Employing [3], we quantitatively simulate different $\Delta\lambda_{MR}$ slopes for the fundamental TE mode (TE_{00}) in Fig. 2(a), where $t = 220$ nm and $t_{sl} = 90$ nm. We consider both passive and active MRs based on using strip and ridge waveguides, respectively. Results indicate that the impacts of the variations in w and t on the $\Delta\lambda_{MR}$ are different. For example, passive MRs with w >≈360 nm are more tolerant against width variations compared to thickness variations. The optical mode confines better in the waveguide core as w increases, and hence the variations in w have less impact on the mode distribution. Fig. 2(b) indicates $\Delta^T\lambda_{MR}$ in passive and active MRs. Note that the z-axis denotes $\frac{\Delta^T\lambda_{MR}}{\sigma_t}$. Given an $\alpha_{p/a}$, $\Delta^T\lambda_{MR}$ decreases with an increase in w (better optical mode confinement), and this reduction is significant for w >450 nm, where the waveguide transits from single-mode to multi-mode. Given a waveguide width in Fig. 2(b), $\Delta^T\lambda_{MR}$ rises with an increase in $\alpha_{p/a}$. When $\alpha_{p/a}$ increases, more variations are introduced to the MR, resulting in a higher $\Delta^T\lambda_{MR}$.

Considering Figs. 2(a) and 2(b), when w increases, the

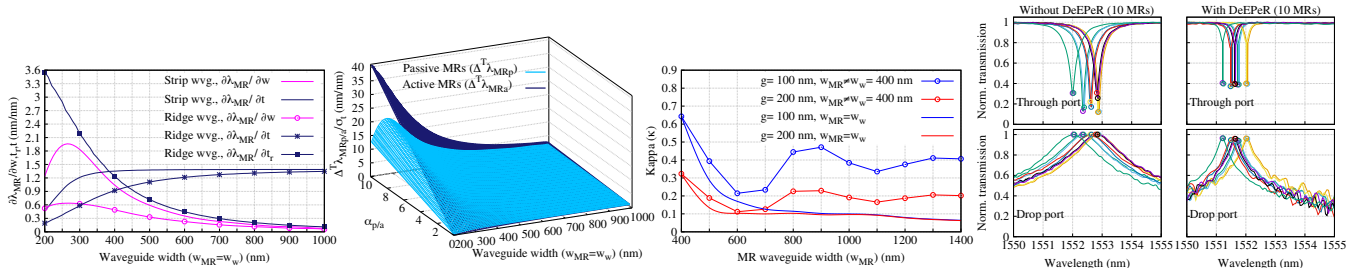

(a) $\Delta\lambda_{MR}$ slopes in passive/active MRs (b) $\Delta^T\lambda_{MR}$ (c) TE_{00} cross-over coupling coefficient (d) Fabrication results ($w_{MR} = w_w$)

Fig. 2. (a) and (b) $\Delta\lambda_{MR}$ slopes and the total shift $\Delta^T\lambda_{MR}$ in passive and active MRs for different waveguide widths (see Fig. 1) when $t = 220$ nm and $t_{sl} = 90$ nm; (c) Cross-over coupling coefficient in a 10 μm passive MR; and, (d) EBeam fabrication results without and with DeEPeR (20 passive MRs).

impact of waveguide width variations is negligible and thickness variations are the dominant contributor to $\Delta^T\lambda_{MR}$. Also, $\Delta^T\lambda_{MR}$ is higher for w <450 nm and its improvement is negligible when w >800 nm (design guideline (DG1)). Avoiding the excitation of higher order modes when w >450 nm, we propose using waveguide tapers, also required for waveguide bendings and the MR curvature (DG2). Employing multi-mode waveguides also impacts the coupling efficiency in MRs [4]. Fig. 2(c) indicates TE_{00} cross-over coupling coefficient (κ) in a 10 μm passive MR, and when the input waveguide width (w_w, see Fig. 1) and the MR waveguide width (w_{MR}) are the same and different. While $w_{MR} = w_w$ results in a poor coupling, κ reaches its second maximum (≈20% lower) when $w_{MR} \approx 2w_w$ (DG3) ($w_w = 400$ nm is considered as an example in Fig. 2(c)). To summarize, depending on the expected range of variations ($\alpha_{p/a}$), DeEPeR optimizes MRs design, minimizing $\Delta^T\lambda_{MR}$ based on $w \in$[450, 800] nm (when $t = 220$ nm), and $\kappa \geq \kappa'$, where κ' is a minimum coupling required in the MR under design. Note that κ can be improved considering different gaps and $w_{MR} \neq w_w$ (see Fig. 2(c)). DeEPeR design guidelines (DG1-3) can be implemented in a design automation tool to facilitate finding the optimum w as well as MR layout creation and verification.

III. Fabrication and Simulation Results

Two TE-polarized passive MR-based add-drop filters (without and with DeEPeR) are designed, ten identical copies of each were placed on a 1.2×0.8 mm^2 chip fabricated by EBeam lithography at Applied NanoTools Inc. (ANT). All MRs are 6.1 μm in radius and designed to resonate at 1550 nm. According to DG1, we assess the impact of DeEPeR on $\Delta^T\lambda_{MR}$ at the proposed w range lower and upper bounds. As a result, we consider $w_{MR} = w_w = 400$ nm with $g = 200$ nm without DeEPeR, and $w_{MR} = w_w = 800$ nm with $g = 100$ nm with DeEPeR, while $t = 220$ nm. Note that $g = 100$ nm is considered to improve the coupling when using DeEPeR. The measured through and drop port responses around 1550 nm are indicated in Fig. 2(d). Thermal variations are eliminated during testing the chip. The resonant peaks (specified by circles) are much closer to the designed resonance with DeEPeR. On average, $\Delta^T\lambda_{MR}$ is 2.6 nm without DeEPeR, and it reduces to 1.6 nm with DeEPeR. $\Delta^T\lambda_{MR}$ can be as small as only 1 nm with DeEPeR, while it is as worse as 3 nm without using DeEPeR. Note that the drop port response with DeEPeR is slightly noisier due to a weaker coupling, which can be

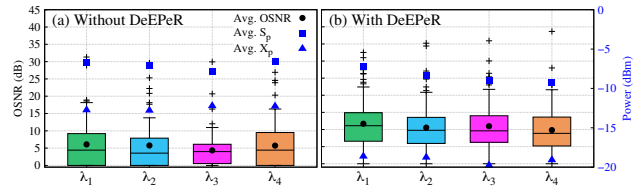

Fig. 3. The OSNR (box-plots) associated with different optical wavelengths on the drop port of the passive optical filter in Fig. 1(b) under 100 different PV maps: (a) Without using DeEPeR and (b) When DeEPeR is applied.

improved using $w_{MR} \approx 2w_w$. The data from ANT indicates that $\alpha_p < 1$, under which $\Delta^T\lambda_{MRp}$ slightly improves when w increases from 400 to 800 nm (see Fig. 2(b)).

We apply DeEPeR to the passive WDM optical filter in Fig. 1(b), and evaluate the OSNR associated with each optical wavelength (λ_i and $i = 1$ to 4). The MR parameters discussed for the fabrication, and $\lambda_{MR1} = 1550$ nm with a channel spacing of 4 nm are considered. The optical power for each λ_i on the input port is 0 dBm. The OSNR associated with λ_i is defined as $10\log_{10}\frac{S_{pi}}{X_{pi}}$, where S_{pi} and X_{pi} are the optical signal and crosstalk power associated with λ_i on the drop port. We assume first-order coherent and incoherent crosstalk noise in our simulations. Given within-die $\sigma_t = 1$ nm and $\sigma_w = 5$ nm [1] and a normal distribution, we randomly generate 100 PV maps, each of which includes different w and t values, and apply them to the MRs in Fig. 1(b). DeEPeR is implemented in our in-house simulator [2], which is also used to calculate S_{pi} and X_{pi}. Results are indicated in Fig. 3(a) (without DeEPeR) and Fig. 3(b) (with DeEPeR). As can be seen, when DeEPeR is employed, $\Delta^T\lambda_{MR}$ is smaller, resulting in a lower average crosstalk noise on the drop port for each λ_i (6.5 dB lower on average), but also some power loss (1.3 dB on average) due to a weaker coupling in MRs. Nevertheless, on average, the OSNR is 5.2 dB (≈3×) higher with DeEPeR.

IV. Conclusion

We demonstrate DeEPeR, an efficient device-level design method based on MRs design space exploration to improve MRs reliability and OSNR in MR-based PICs. DeEPeR is validated through both fabrication and simulation. While DeEPeR can be easily applied to PICs, it helps reduce the tuning power required to correct faulty MRs in PICs.

References

[1] L. Chrostowski *et al.*, in *OFC*, 2014, paper Th2A.37.
[2] M. Nikdast *et al.*, *IEEE JLT*, vol. 34, no. 16, pp. 3682–3695, 2016.
[3] Lumerical Solutions, Inc. http://www.lumerical.com/tcad-products/mode/.
[4] Y. Luo *et al.*, *IEEE PLT*, vol. 28, no. 13, pp. 1391–1394, 2016.